Anaerobic Neutrophilic Pyrite Oxidation by a Chemolithoautotrophic Nitrate-Reducing Iron(II)-Oxidizing Culture Enriched from a Fractured Aquifer

Natalia Jakus, Adrian Mellage, Carmen Höschen, Markus Maisch, James M. Byrne, Carsten W. Mueller, Peter Grathwohl, and Andreas Kappler*

Read Online

ACCESS | Metrics & More | Article Recommendations | Supporting Information

ABSTRACT: Neutrophilic microbial pyrite (FeS_2) oxidation coupled to denitrification is thought to be an important natural nitrate attenuation pathway in nitrate-contaminated aquifers. However, the poor solubility of pyrite raises questions about its bioavailability and the mechanisms underlying its oxidation. Here, we investigated direct microbial pyrite oxidation by a neutrophilic chemolithoautotrophic nitrate-reducing Fe(II)-oxidizing culture enriched from a pyrite-rich aquifer. We used pyrite with natural abundance (NA) of Fe isotopes (^{NA}Fe-pyrite) and ^{57}Fe-labeled siderite to evaluate whether the oxidation of the more soluble Fe(II)-carbonate ($FeCO_3$) can indirectly drive abiotic pyrite oxidation. Our results showed that in setups where only pyrite was incubated with bacteria, direct microbial pyrite oxidation contributed ca. 26% to overall nitrate reduction. The rest was attributed to the oxidation of elemental sulfur (S^0), present as a residue from pyrite synthesis. Pyrite oxidation was evidenced in the ^{NA}Fe-pyrite/^{57}Fe-siderite setups by maps of ^{56}FeO and ^{32}S obtained using a combination of SEM with nanoscale secondary ion MS (NanoSIMS), which showed the presence of ^{56}Fe(III) (oxyhydr)oxides that could solely originate from ^{56}FeS$_2$. Based on the fit of a reaction model to the geochemical data and the Fe-isotope distributions from NanoSIMS, we conclude that anaerobic oxidation of pyrite by our neutrophilic enrichment culture was mainly driven by direct enzymatic activity of the cells. The contribution of abiotic pyrite oxidation by Fe^{3+} appeared to be negligible in our experimental setup.

KEYWORDS: *denitrification, siderite oxidation, NRFeOx, anoxic subsurface*
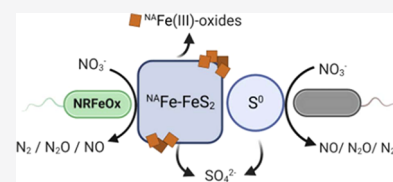
INTRODUCTION

In low-oxygen environments, nitrate can be naturally attenuated via denitrification or dissimilatory nitrate reduction to ammonium (DNRA). Among several environmental factors controlling the dominant nitrate removal pathway, carbon limitation in the presence of excess nitrate has been shown to favor denitrification.[1−3] Denitrification is the stepwise reduction of nitrate via nitrite (NO_2^-), nitric oxide (NO), and nitrous oxide (N_2O) to dinitrogen gas (N_2), where each step can be catalyzed by microbes equipped with specific reductase enzymes.[4] While organic matter oxidation yields the most energy, in many ecosystems, the availability of organic carbon is limited and inorganic compounds become alternative electron donors for denitrifiers.[5] These chemolithoautotrophic bacteria produce energy for CO_2 fixation from the reduction of nitrate coupled to oxidation of compounds such as reduced sulfur species or Fe(II).[6,7]

In anoxic, circumneutral pH environments, Fe(II) can be found as dissolved Fe^{2+}, complexed by organic matter (Fe(II)-OM),[8,9] or adsorbed onto mineral surfaces. However, Fe(II) is predominantly embedded within the structure of Fe(II)-rich clays or minerals like siderite ($FeCO_3$) and pyrite (FeS_2).[10] Denitrification at neutral pH coupled to Fe(II) sulfide oxidation has been examined extensively in many environ-

ments such as surface sediments,[11] marine sediments,[12] freshwater wetlands, and coastal sites,[13] and in different types of aquifers like sandy,[14−16] schist,[17] and clay and gravel[18] aquifers. Pyrite oxidation has been also proposed recently to drive denitrification in a fractured carbonate aquifer.[18,19] The mechanisms enabling pyrite-mediated denitrification, however, remain a matter of contention in the literature, with several studies arriving at contradictory conclusions.[20] The ambiguity in the current process understanding hints at a more complex picture than currently thought. For instance, nitrate reduction, which was previously attributed to pyrite oxidation, may also occur as a result of oxidation of intracellularly stored sulfur or residual elemental sulfur that typically is associated with synthetized FeS_2.[20]

In pH-neutral environments, pyrite oxidation can be coupled to the abiotic reduction of two other oxidants: O_2 and Fe(III).[21] Indeed, isotopic evidence has provided support for

anaerobic FeS_2 oxidation with Fe(III) as an oxidant in marine sediments.[22] Although both reactions occur abiotically, parallel microbially mediated reactions can enhance the kinetics and extent of pyrite weathering. In a study investigating subglacial habitats, chemolithotrophic bacteria were found to oxidize pyrite using oxygen in carbonate-buffered system.[23] Similarly, in another study, an enrichment culture was shown to increase rates of pyrite oxidation under oxic pH-neutral conditions by an order of magnitude compared to abiotic rates.[24] Microorganisms were also proposed to be indirectly involved in a Fe(III)-driven pyrite oxidation pathway.[25] In this "indirect" mechanism, enzymatic oxidation of aqueous Fe^{2+} resulted in the formation of Fe^{3+} ions that abiotically oxidized pyrite, yielding a release of sulfate and regeneration of aqueous Fe^{2+} that can be further oxidized microbially. This mechanism is, however, limited by the immediate precipitation of Fe^{3+}.[12,26] The direct attachment of cells onto the surface of pyrite, however, can lead to the formation of a slightly acidic pH microenvironment at the cell−mineral interface or the release of organic ligands, which may increase pyrite dissolution and oxidation rates.[24−26] One remaining question is whether in anoxic environments, nitrate can substitute O_2 and serve as an electron acceptor for direct or indirect pyrite oxidation.

The primary goal of this study was therefore to determine if, at neutral pH, autotrophic bacteria can mediate pyrite oxidation and couple it to the reduction of nitrate either by direct or indirect pyrite oxidation. We incubated a lithoautotrophic nitrate-reducing Fe(II)-oxidizing (NRFeOx) culture, which was enriched using Fe(II)-rich crushed limestone particles exposed to groundwater, in a nitrate-containing medium with siderite and/or pyrite. Combining geochemical monitoring of dissolved species and HCl-extractable iron with a reaction model, we determined the relative contributions of the dominant reaction mechanisms driving denitrification coupled to solid-phase Fe(II) oxidation. We also identified the mineral products and their spatial associations using nanoscale secondary ion MS (NanoSIMS) in combination with SEM, Mössbauer spectroscopy, and ^{57}Fe-labeled (100%) siderite to differentiate them from nonlabeled pyrite and pyrite-derived oxidation products with naturally abundant iron isotopes, including ^{56}Fe (2.20%) that was used as an isotopic marker.

■ MATERIALS AND METHODS

Preparation and Characterization of Iron Minerals. ^{57}Fe-siderite and ^{NA}Fe-siderite (natural abundance of Fe isotopes) were synthetized and characterized as described in the Supporting Information. Synthesized pyrite was boiled in 1 M HCl for 1 h and then washed 3 times with MQ water, 3 times with acetone, and 10 times with petroleum ether to remove residual unreacted elemental sulfur following the protocol described by Yan et al.[20] The final ^{NA}Fe-pyrite contained 3.12 ± 0.1 mass % elemental sulfur (determined by HPLC, see the Supporting Information), which was slightly lower than the 4.6 mass % elemental sulfur reported by Yan et al.[20]

Cultivation of Microorganisms. A chemolithoautotrophic NRFeOx culture was enriched from an anoxic, pyrite-rich limestone aquifer in southwest Germany.[27] Before the experiments, the culture was pre-grown in an anoxic bicarbonate-buffered (22 mM) freshwater low-phosphate medium (LPM) modified from Ehrenreich & Widdel[28] containing 0.6 g/L KH_2PO_4, 0.3 g/L NH_4Cl, 0.5 g/L

$MgSO_4 \cdot 7H_2O$, and 0.1 g/L $CaCl_2 \cdot 2H_2O$, adjusted to pH 7.0−7.1, and supplemented with 2 mM $NaNO_3$ and 2 mM $FeCl_2$ as described in detail in the Supporting Information. 16S rRNA gene sequencing revealed that the culture consists of microorganisms that are related to bacteria previously reported in pyrite-oxidizing and nitrate-reducing communities, such as *Gallionellaceae* sp., *Acidovorax* sp., and *Thiobacillus denitrificans*.[27]

Batch Pyrite Oxidation Experiments. Batch pyrite oxidation experiments were conducted at 25 °C in serum glass bottles (58 mL volume, 25 mL medium) sealed with butyl rubber stoppers and flushed with CO_2/N_2 (20/80%) (Figure S2). A bicarbonate-buffered (22 mM, pH 7.0) LMP medium was prepared for precultivation (Supporting Information). All experimental setups were amended with 2 mM $NaNO_3$. In three different biotic setups, either (1) ^{57}Fe-siderite, (2) ^{NA}Fe-pyrite, or (3) ^{NA}Fe-pyrite and ^{57}Fe-siderite were added to reach concentrations of 2, 5, and 7 mM total Fe(II), respectively. Additionally, another biotic experiment was conducted with (4) both ^{NA}Fe-pyrite and ^{NA}Fe-siderite as a control for isotopic enrichment in siderite. All biotic setups were inoculated with 10% (vol/vol) of the NRFeOx enrichment (ca. 2×10^6 cells mL^{-1}). Two abiotic controls containing both ^{NA}Fe-pyrite and ^{57}Fe-siderite were prepared: (5) with 10% autoclaved cells to determine the potential influence of the presence of inactive cells and (6) without cells to assess a potential isotopic exchange between pyrite and siderite. All experiments were run in triplicate.

Sampling and Chemical Analysis. Batch incubations were sampled in an anoxic glovebox (100% N_2) by withdrawing 0.4 mL aliquots using sterile syringes. Samples were centrifuged (14,000g, 10 min) to separate the supernatant from iron minerals and biomass. Samples for nitrate, nitrite, and sulfate analyses were diluted in anoxic MQ and stored anoxically until measurements were performed. Nitrate and nitrite were quantified following the DIN 38405/ISO 13395 standard quantification method using an AA3 HR AutoAnalyzer System (Seal Analytical, Germany) equipped with a dedicated dialysis membrane delivered by the manufacturer to eliminate potential interference with any solids that could remain in the samples after centrifugation. Sulfate was measured by ion chromatography (Eco IC, Metrohm). Samples containing dissolved Fe^{2+} were diluted with anoxic 1 M HCl to prevent oxidation and analyzed using the ferrozine method.[29,30] Treatment and analyses of the solid phase are described in the Supporting Information.

Conceptual and Numerical Reaction Models. Based on the results from our incubation experiments, we postulated two competing conceptual models to qualitatively and quantitatively describe the measured geochemical data (Figure 1). Scenario 1 (S1) assumes that oxidation of all available solid-phase electron donors (siderite, pyrite, and S^0) is independently biologically catalyzed, coupled to the reduction of nitrate, and does not consider additional reversible redox feedback loops (Figure 1A,C,D). Scenario 2 (S2), in addition to all processes listed in S1, includes the possibility of abiotic pyrite oxidation by Fe^{3+}, produced from siderite oxidation. The additional abiotic step releases Fe^{2+} (and $SO_4^{2−}$) into the solution, providing more available electron donor that can contribute to sustain nitrate reduction, by closing the Fe-redox cycle (Figure 1E).

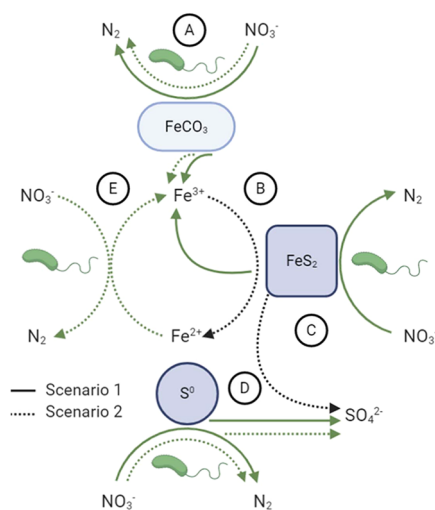We formulated our conceptual model(s) into a reaction model, assuming well-mixed conditions without explicitly

Figure 1. Conceptual figure showing a network of abiotic (black lines) and bacterially mediated reactions (green lines) that might lead to nitrate removal: microbial siderite oxidation coupled to nitrate reduction (A), abiotic pyrite oxidation coupled to Fe^{3+} reduction (B), microbial pyrite oxidation coupled to nitrate reduction (C), microbial elemental sulfur oxidation coupled to nitrate reduction (D), and microbial Fe^{2+} oxidation coupled to nitrate reduction (E). The two different line types represent two scenarios modeled in this study. Scenario 1 (S1, solid lines) includes reactions A, C, and D and represents a model where oxidation of all available electron donors, i.e., siderite, pyrite, and elemental sulfur, happened independently from each other, with nitrate serving as the electron acceptor (panels A, C, and D). Scenario 2 (S2, dashed lines) includes (in addition to the processes in S1) the abiotic oxidation of In turn, pyrite oxidation produces Fe^{2+}, which can be microbially oxidized and form Fe^{3+} again closing the feedback loop (E). The models assume that denitrification and sulfur oxidation are complete, leading to formation of N_2 and SO_4^{2-}, respecively. Created with BioRender.com.

considering mineral surface interactions such as the sorption of Fe(III) onto pyrite prior to pyrite oxidation. The model, written in MATLAB and described in detail in the Supporting Information, assumes that nitrate is reduced to N_2 and that reduced sulfur species (S_2^{2-} and S^0) are oxidized to SO_4^{2-}. In our model, both oxidation of pyrite and oxidation of S^0 contribute to the total SO_4^{2-} pool. The S1 formulation of our simplified model was calibrated jointly to the experimental data of the siderite- and pyrite-only incubations, as these allowed to separate the reactive contributions of siderite and pyrite from one another, which were then lumped in a validation step of the "mixed" experiment, thus allowing us to propose potentially dominant reaction pathways based on quantitative rate law formulations.

SEM and NanoSIMS Imaging. Samples (100 μL) for SEM and NanoSIMS were withdrawn with a syringe in an anoxic glovebox (100% N_2) from the treatments containing (1) ^{NA}Fe-pyrite, ^{57}Fe-siderite, and bacterial cells, (2) ^{NA}Fe-pyrite, ^{NA}Fe-siderite, and bacterial cells, and (3) ^{NA}Fe-pyrite, ^{57}Fe-siderite, and autoclaved bacterial cells. Each sample was mixed with 400 μL of 0.2 μm-filtered anoxic MQ water. Thereafter, an aliquot of 60 μL was loaded on a silica wafer and left until dry in the glovebox. The wafers were mounted on SEM stubs and stored anoxically until sputter-coated with Pd (~12 nm). To characterize the distribution and spatial relation between pyrite, siderite, and Fe(III) (oxyhydr)oxides, an SEM system (JEOL JSM-6500F field emission SEM) with a

Schottky field emitter (JEOL Ltd., Japan), equipped with a secondary electron detector (acceleration voltage of 10 kV; working distance of 5.29 mm), was used. NanoSIMS analyses were performed using a Cameca NanoSIMS to map the distribution of siderite and pyrite products revealed by the secondary ions ^{56}Fe, ^{57}Fe (O^- primary beam, a radio frequency (RF) source) and ^{56}FeO, ^{32}S (Cs^+ primary beam). The measuring procedure and parameters are described in the Supporting Information.

■ RESULTS AND DISCUSSION

Nitrate Attenuation. To determine the extent of oxidation of Fe(II) minerals coupled to nitrate reduction, we incubated an autotrophic NRFeOx enrichment culture with siderite, pyrite, or a mix of both minerals and followed concentrations of NO_3^-, SO_4^{2-}, and HCl-extractable Fe(II)/Fe(III) over time (Figure 2). The abiotic treatment exhibited negligible nitrate reduction indicated by NO_3^- concentrations that remained constant throughout the experiment (Figure 2A and Table S2). Conversely, in all biotic treatments, NO_3^- exhibited a significant drop from the starting 2 mM concentrations, indicating that biological activity mediated denitrification either in the presence of only siderite, only pyrite, or a mixture of pyrite and siderite. During 146 day incubation in the presence of ^{57}Fe-siderite (no pyrite), the autotrophic NRFeOx enrichment culture reduced 0.16 ± 0.13 mM NO_3^- (Figure 2A and Table S2). The reduction started right after inoculation and lasted until day 4 with an average integrated nitrate reduction rate of 0.05 ± 0.01 mM day^{-1}. No further changes in NO_3^- concentrations were measured after day 4. In contrast, in microcosms with only pyrite, the concentration of nitrate decreased steadily from 2 to 1.2 mM, leveling off to a constant value at day 27, yielding an integrated consumption of 0.79 ± 0.19 mM nitrate over the 146 day incubation. In the presence of both pyrite and ^{57}Fe- or ^{NA}Fe-siderite, the NRFeOx culture reduced 0.84 ± 0.04 and 0.90 ± 0.06 mM nitrate in 146 days, respectively. Nitrate reduction commenced without a detectable lag phase. Analogous to the pyrite-only treatment, NO_3^- concentrations dropped steadily from 2 to 1 mM until day 27. In both setups, no further changes in nitrate were observed thereafter. The amount of nitrate reduced in all pyrite-containing microbially active batches was higher than the amount of nitrate that can be reduced by this culture when no electron donors are supplied to the medium (0.24 ± 0.06 mM nitrate consumption). This background nitrate consumption is probably due to the oxidation of substrates that are carried over from the preculture, stored within cells, or organic carbon background present in MQ water used to prepare the microbial medium, as it was previously discussed by Jakus *et al.*[27] Therefore, most of nitrate reduction observed in our inoculated experiments can be attributed to microbial oxidation of siderite, pyrite, and traces of elemental sulfur.

Sulfate Formation and $Fe^{2+}_{(aq)}$ Release. The abiotic experiments containing siderite and pyrite and the biotic incubations with ^{57}Fe-siderite (no pyrite) exhibited a minor increase in SO_4^{2-} concentrations between day 0 and 10, resulting probably from measurement errors, which was followed by a drop to the initial SO_4^{2-} concentration (Figure 1B). Therefore, we conclude that in abiotic controls and batches containing ^{57}Fe-siderite (no pyrite), there were no changes in SO_4^{2-} concentrations during the experiment. In experiments where both ^{NA}Fe-pyrite and ^{57}Fe-siderite or ^{NA}Fe-pyrite and ^{NA}Fe-siderite were incubated, 0.61 ± 0.08 mM
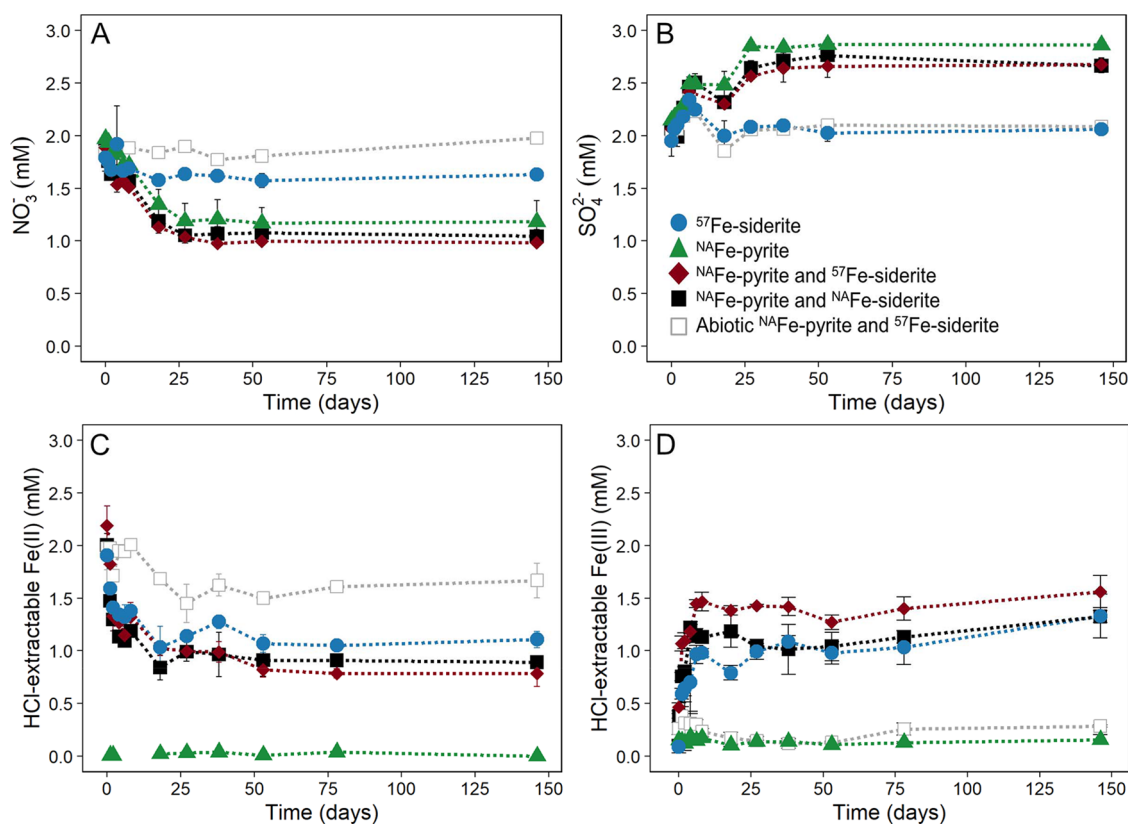
Figure 2. Nitrate (A), sulfate (B), HCl-extractable Fe(II) (C), and Fe(III) concentrations (D) in setups where the autotrophic NRFeOx enrichment culture was incubated with nitrate and ^{57}Fe-siderite (blue circles), ^{NA}Fe-pyrite (green triangles), and both ^{NA}Fe-pyrite and either ^{57}Fe-siderite (black squares) or ^{NA}Fe-siderite (red diamonds) under anoxic, pH-neutral conditions. Abiotic controls contained 10% vol of the same culture that was inactivated by autoclaving. All data points are average values of samples from three independent biological replicates; error bars represent standard deviations. Please note that the higher sulfate concentration measured at day 10 in all samples (panel B) resulted from an analytical problem at the ion chromatograph. Additional plots of the data for the first 30 days can be found in the Supporting Information (Figure S3).

sulfate and 0.60 ± 0.07 mM sulfate were produced between day 0 and day 27, respectively. The highest concentration of sulfate appeared in the setups with only pyrite (0.72 ± 0.2 mM; Table S2). In all setups, no accumulation of dissolved Fe^{2+} was observed (Table S2) since all available Fe^{2+} was most probably immediately consumed by microbes. This can be supported by accumulation of Fe^{2+} in the abiotic control containing pyrite and ^{57}Fe-siderite, where 0.21 ± 0.02 mM Fe^{2+} originating from dissolution of minerals was measured after 146 days. We speculate that the accumulation was due to the lack of Fe(III) precipitates that would have otherwise sorbed Fe(II). To quantify the concentration of Fe^{2+} that could potentially adsorb to mineral particles and serum bottle glass walls, we further measured HCl-extractable Fe(II) (see the next section).

Fe(II) Oxidation and Formation of Fe(III) (Oxyhydr)-oxides. Using 1 M HCl, we extracted all HCl-soluble Fe(II), mainly derived from siderite together with Fe(II) potentially sorbed to the surface of Fe(III) (oxyhydr)oxide minerals. The synthetized pyrite was insoluble in 1 M HCl; therefore, Fe(II) originating from pyrite was not quantified using this method. We found that in all biotic setups containing siderite, a concentration of total HCl-extractable Fe(II) (2 mM) rapidly decreased by 27.4−48.7% within the first 8 days (Figure 2C). In the setups containing siderite with or without pyrite, a fraction of the HCl-extractable Fe(II) was converted to HCl-extractable Fe(III) (Figure 2D). Specifically, in incubations

where only siderite (2 mM) was present, our ferrozine spectrophotometric analyses showed that the concentration of HCl-extractable Fe(II) decreased by 0.78 ± 0.01 mM, while 1.28 ± 0.2 mM HCl-extractable Fe(III) was formed (Table S2). This suggests that some of the "missing" Fe(II) either transformed to more stable Fe(II) phases nondissolvable in 1 M HCl (after 1 h extraction at room temperature) such as magnetite, or, probably more likely, sorbed to the walls of the glass bottles since our mineral analyses did not show evidence for magnetite (see below).[31]

In incubations containing both pyrite and ^{57}Fe-siderite or pyrite and ^{NA}Fe-siderite, slightly more Fe(II) was depleted (removal of 1.11 ± 0.08 and 1.40 ± 0.14 mM Fe(II), respectively) than Fe(III) formed (0.94 ± 0.07 and 1.09 ± 0.14 mM Fe(III) formed, respectively) (Table S2). In the abiotic setups, the concentration of HCl-extractable Fe(II) decreased by 0.31 ± 0.29 over time of the experiment, but no Fe(III) was formed, hence supporting our hypothesis of Fe(II) loss via siderite dissolution, as evidenced by the presence of Fe^{2+}(aq), followed by Fe(II) adsorption to the glass walls of the incubation bottles (Table S2). This is further supported by the total HCl-extractable Fe(II)/Fe(tot) ratio (Figure S2), where the abiotic control remained stable over the complete time of incubation.

Reaction Model Results. Reaction model-simulated concentration time series were compared to experimental data obtained from the siderite-only, pyrite-only, and the
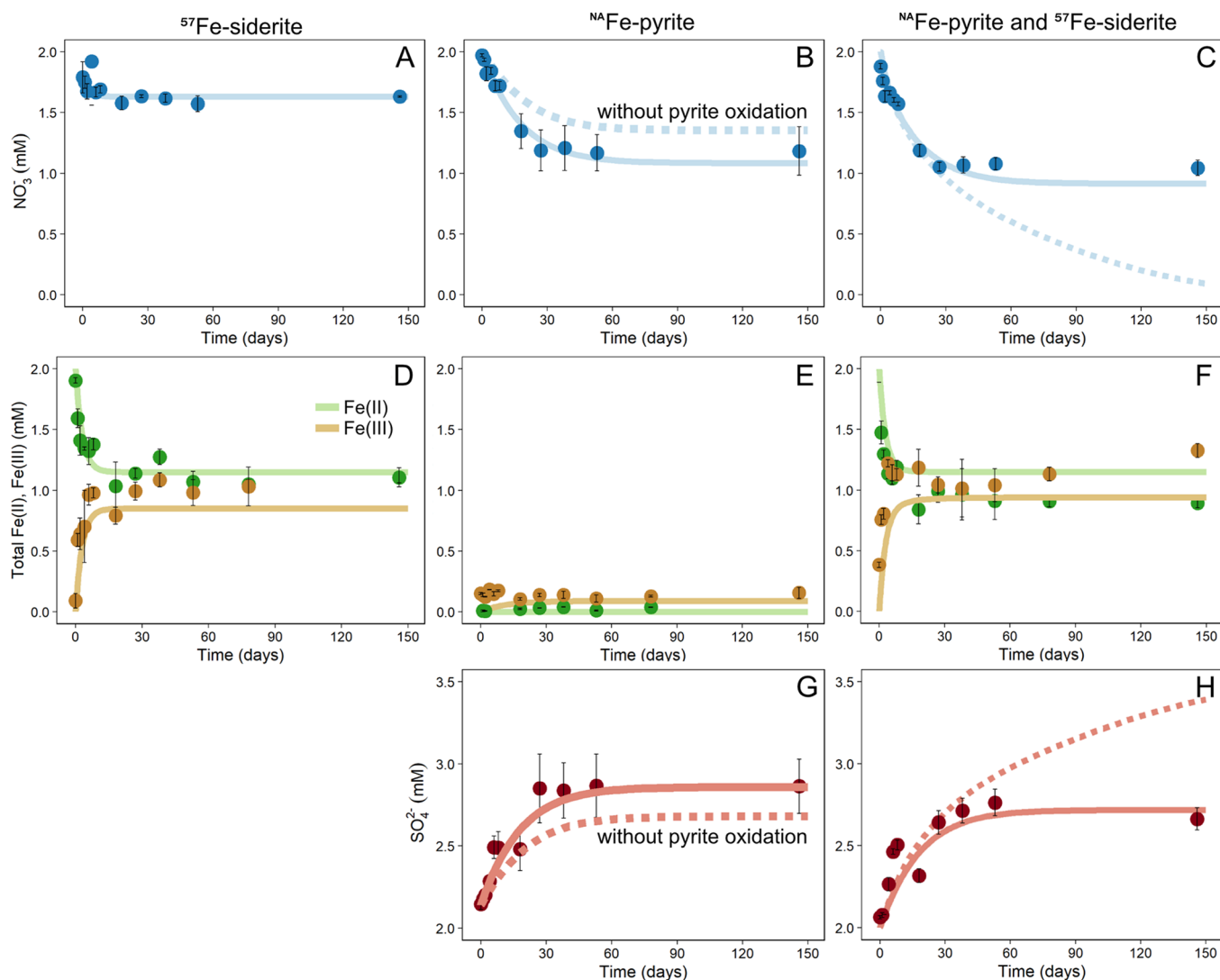
Figure 3. Simulation results (lines) and experimental data (circles) showing nitrate (first row), iron (second row), and sulfate (third row) concentrations in three experimental setups where the autotrophic NRFeOx culture was incubated with nitrate and ^{57}Fe-siderite (first column), ^{NA}Fe-pyrite (second column), and both ^{NA}Fe-pyrite and ^{57}Fe-siderite (third column) under anoxic, pH-neutral conditions (A−H). Dashed lines in panels B and G correspond to the case where no pyrite oxidation takes place but instead, nitrate is reduced by oxidation of elemental sulfur, leading to formation of sulfate. Dashed lines on panels C, F, and H represent scenario 1, which, in addition to reactions simulated in S1, includes the feedback loop of abiotic pyrite oxidation by Fe^{3+}.

mixed pyrite/siderite incubations (Figure 3). (Note: The "mixed" model output was compared to the dataset collected using isotopically labeled siderite). For both the siderite- and pyrite-only cases, the simulated concentrations of all species aligned well with measurements (Figure 3). However, the model slightly underestimated the final amount of Fe(III) formed in the siderite incubation, likely related to the issue with Fe quantification discussed in the section above. In addition to the model output accounting for direct biotic pyrite oxidation, we also plotted the output of a version that excluded biotic pyrite oxidation and only accounted for sulfur-dependent denitrification to test whether concentration time series could be matched based on the presence of elevated levels of S^0 alone (see dashed lines in Figure 3B,G). Despite the large amount of S^0, the inclusion of microbial pyrite oxidation best fit the results, supporting our conceptual model that direct microbial pyrite oxidation contributed to nitrate reduction (Figure 3B) (and sulfate formation, Figure 3G). Thus, when comparing scenarios S1 and S2 in the mixed case, we

considered biotic pyrite oxidation in both. The solid lines in Figure 3C,F,G are the model-simulated concentrations for S1, considering mixed biotic siderite and pyrite oxidation and S^0-mediated denitrification. The combined reactions of the siderite oxidation and pyrite oxidation alone (S1) adequately captured the time series behavior of nitrate, Fe(II)/Fe(III), and sulfate. Conversely, the inclusion of an additional feedback loop, S2 (dashed lines in Figure 3C,H), led to an over-estimation of nitrate consumption and sulfate production. Meaning that iron(II) released from the abiotic oxidation of pyrite would lead to more denitrification and sulfate production than those measured. Instead, the reaction was limited and most of the reduction stopped at around day 30 (Figure 3A). The reaction was most probably constrained by the rapid precipitation of Fe^{3+} as Fe(III) (oxyhydr)oxides (discussed below), suggesting that siderite-mediated pyrite oxidation played a negligible role in our experiments.

Relative Abundance and Identity of Solid Phases. Mössbauer spectroscopy was used to follow the fate of pyrite

and to identify the products of Fe(II) oxidation formed during the experiment. In the setup where both pyrite and ^{57}Fe-siderite were present, the initial relative abundances of siderite and pyrite were 94.2 and 5.2%, respectively (Figure 4). The
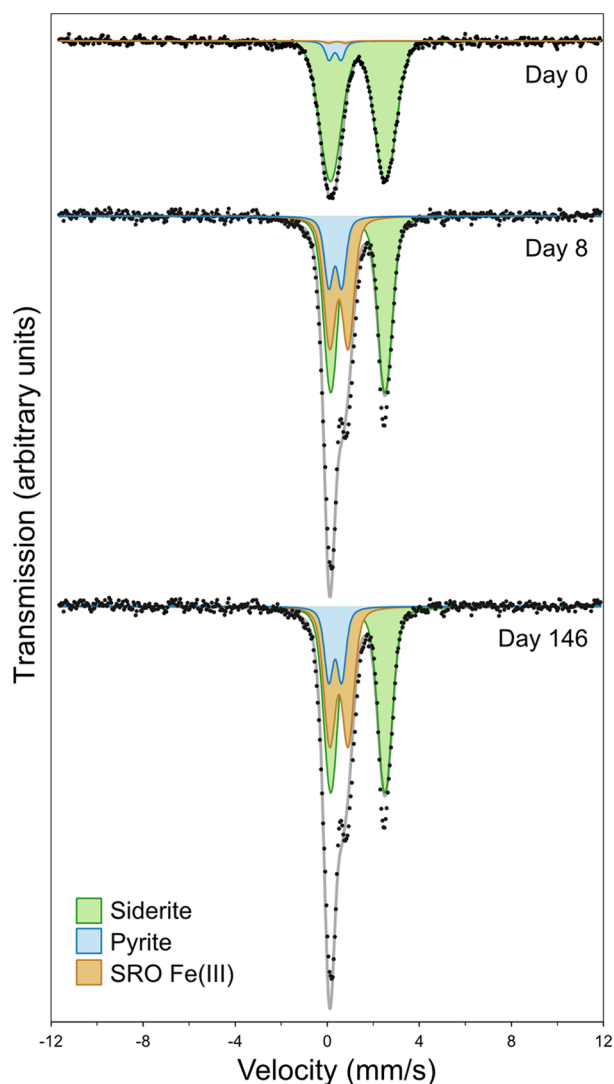

Figure 4. Mössbauer spectra (collected at 77 K) of setups containing both pyrite and siderite at the beginning of the experiment (day 0), during incubation (day 8), and at the end of the experiment (day 146) showing the formation of short-range ordered (SRO) Fe(III) phases as a result of oxidation induced by the autotrophic NRFeOX culture. Black dots represent raw data, the gray line shows the fitted spectrum, the green shading represents siderite, and blue indicates pyrite, while the brown area represents SRO Fe(III), likely ferrihydrite.

sample contained also a small amount of a short-range ordered Fe(III) phase (SRO) (0.6%), likely Fe(III) (oxyhydr)oxides, which most probably was transferred together with bacterial cells from the preculture (Figure 4). In samples collected after 8 and 146 days of incubation, we observed an increase in the relative abundance of the SRO Fe(III) phase to up to 33.1 and 43.4%, respectively. Considering a balance of relative phase abundances from day 0 to 146, the Voigt-based fitting (VBF) models (see the Supporting Information) suggest a predominant shift in phases from ^{57}Fe-siderite to SRO Fe(III) phases (Figure 4 and Table S3), which can be attributed to the

formation of, e.g., ferrihydrite. Due to the low relative abundance of ^{57}Fe originating from pyrite (natural enrichment, ca. 2.2%) compared to ^{57}Fe originating from siderite (100% enrichment), pyrite oxidation evidenced by our geochemical and modeling data (see above) could be neither confirmed nor denied using the Mössbauer data. Furthermore, other highly crystalline Fe(II)-Fe(III) phases, insoluble in 1 M HCl after 1 h extraction at room temperature, that could potentially form in our setups (e.g., magnetite) were not detected. Finally, since the relative abundances of pyrite and siderite (in the abiotic setup) in the ^{57}Fe-specific Mössbauer spectrum did not change during incubation (Table S3), there was no isotopic exchange between ^{57}Fe-siderite and pyrite. This was a relevant control for the later NanoSIMS investigations, i.e., it allowed us to use ^{57}Fe from siderite to follow the formation of ^{57}Fe(III) as consequence of ^{57}Fe-siderite oxidation.

Spatial Distribution of Pyrite, Siderite, and Formed Fe(III) (Oxyhydr)oxides. SEM images of samples collected on day 8 of the incubation showed that mineral aggregates consisted of phases with various morphologies reflecting the presence of both pyrite and siderite (abiotic controls, Figure S3A) or pyrite, siderite, and Fe(III) (oxyhydr)oxides (biotic controls, Figure 5A and Figure S3B). By NanoSIMS, we
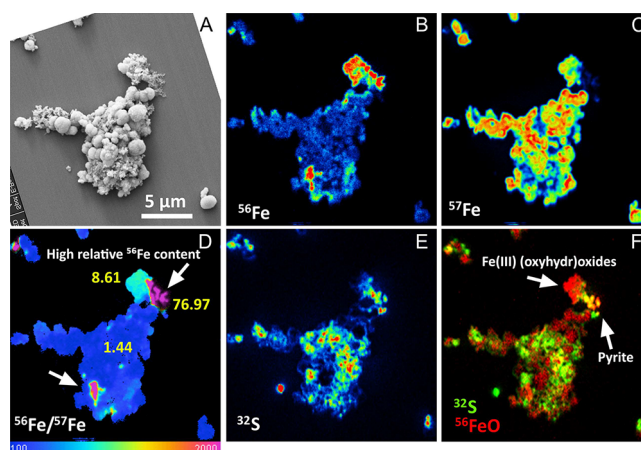

Figure 5. SEM image of a mineral aggregate (A) together with high spatial resolution NanoSIMS analysis of two isotopes of iron: ^{56}Fe (B) and ^{57}Fe (C) along with a ratio image of ^{56}Fe/^{57}Fe showing areas enriched in ^{56}Fe (D, arrows). Average ^{56}Fe/^{57}Fe ratios are shown next to the investigated areas (D, yellow font). Further, ^{32}S distribution (E) and composite images of ^{32}S and ^{56}FeO (E) are shown. All images were collected at the 8th day of incubation of ^{57}Fe-siderite and ^{NA}Fe-pyrite with the NRFeOx culture. ^{57}Fe and ^{56}Fe were used as signatures of siderite and pyrite, respectively. Zones with a high ^{56}Fe/^{57}Fe ratio correlating with the distribution of ^{32}S indicate pyrite, while the absence of sulfur indicates products of pyrite oxidation (Fe(III) (oxyhydr)oxides). ^{56}Fe and ^{57}Fe were measured with an O$^-$ source and ^{32}S and ^{56}FeO with a Cs$^+$ source presenting different distortions. The values on the scale for hyperspectral imaging (HSI) images are multiplied by 10,000.

obtained the spatial distribution of the two iron isotopes: ^{56}Fe (Figure 5A), predominantly originating from pyrite, and ^{57}Fe (Figure 5B), predominantly originating from siderite (purity, 97.83%) and, to a much lower extent, from pyrite (with a natural abundance of ^{57}Fe of 2.12%). We used the ^{56}Fe/^{57}Fe isotopic ratio to identify phases relatively enriched in ^{56}Fe. (Note: This was only possible in samples where ^{57}Fe was used since in nonlabeled setups, the distribution of the ^{56}Fe/^{57}Fe

ratio was homogeneous and close to a theoretical value of 43.28, as shown in Figure S4). Most areas analyzed in the particle associations displayed a mean $^{56}Fe/^{57}Fe$ ratio of 1.44 ± 0.52 (Figure 5D, yellow numbers), which is close to the theoretical value of 2.18 that is expected from setups containing a mixture of 5 mM ^{NA}Fe-pyrite and 2 mM ^{57}Fe-siderite (4.59 mM ^{56}Fe and 2.11 mM ^{57}Fe in total), meaning that minerals containing both isotopes were well mixed and homogeneously distributed. Some areas, however, displayed elevated ratios of $^{56}Fe/^{57}Fe$ (Figure 5D), reflecting local enrichment in ^{56}Fe, which indicated the presence of pyrite itself or of Fe(III) (oxyhydr)oxides stemming from oxidation of pyrite. Please note that all areas with elevated amounts of ^{56}Fe represent a mixture of different phases containing both ^{56}Fe and ^{57}Fe rather than pure ^{56}Fe phases (Figure 5), being a result of precipitation of Fe(III) (oxyhydr)oxides stemming from oxidation of both siderite and pyrite since isotopic exchange between the two minerals did not occur (Table S3). We further investigated the distribution of ^{32}S (Figure 5E) to localize S-containing phases, such as S^0 and pyrite. By comparing the distribution maps of S^0 and ^{56}Fe, we were then able to identify areas where ^{56}Fe was present in the absence of sulfur. This allowed us to localize $^{56}Fe(III)$ (oxyhydr)oxides (^{56}Fe-enriched spots not containing any sulfur), which could only be the products of pyrite oxidation. By the overlay of ^{56}FeO and ^{32}S maps (Figure 5F), we finally confirmed the presence of Fe(III) (oxyhydr)oxides enriched in ^{56}Fe, demonstrating that pyrite oxidation occurred.

Evidence for Anaerobic Pyrite Oxidation by NRFeOx Bacteria. For a long time, *Thiobacillus denitrificans* was the only bacterium described to couple pyrite oxidation to nitrate reduction at neutral pH. However, it was recently shown that *T. denitrificans* does not oxidize pyrite but rather the reduced sulfur that is stored intracellularly or present as a contamination in the pyrite.[20] Here, we provide two lines of evidence in support of anaerobic pyrite oxidation mediated by nitrate-dependent Fe(II)-oxidizing bacteria. First, the overall agreement between the reaction model simulation and experimental results obtained from setups containing only ^{NA}Fe-pyrite (and S^0) supports the conceptual assumption that direct microbial oxidation of pyrite coupled to nitrate occurred in our experiments. Second, NanoSIMS composite maps of ^{56}FeO and S obtained from setups containing both ^{NA}Fe-pyrite and ^{57}Fe-labeled siderite revealed the presence of ^{56}Fe-enriched Fe(III) (oxyhydr)oxides that could stem only from oxidation of $^{56}FeS_2$, thus providing compelling evidence for direct microbial oxidation and implying an enzymatic process. Additionally, based on the modeling results, we demonstrated that in setups where a mix of pyrite and siderite was incubated with the NRFeOx culture, indirect abiotic oxidation of pyrite induced by dissolved Fe^{3+} did not contribute significantly to overall pyrite oxidation. However, our model did highlight that a major process contributing to denitrification in all pyrite-containing treatments was S^0 oxidation (Figure S5E,F). We also observed that, although sufficient electron donors (pyrite and siderite) were available to theoretically reduce all nitrate, the reaction was limited and most of the reduction stopped at around day 30 (Figure 3A). Below, we discuss potential factors limiting this reaction.

Factors Limiting Siderite and Pyrite Oxidation. The theoretical maximum concentration of nitrate that the autotrophic NRFeOx culture could reduce to N_2 in our

experimental setup with both pyrite and siderite was 1.4 mM, assuming that all 7 mM Fe(II) present as both siderite and pyrite was bioavailable. Considering oxidation of the S^0 associated with the pyrite that could be potentially mediated by autotrophic sulfur-oxidizing nitrate-reducing bacteria, another 0.65 mM nitrate could be reduced, meaning that there was enough electron donor present for all nitrate (2 mM) to be reduced in our experiments. However, in setups with both pyrite and ^{NA}Fe-siderite, we observed a reduction of a maximum of 0.90 mM nitrate, suggesting a limited bioavailability of the Fe(II) in siderite and/or pyrite. A bioavailability limitation was parameterized into the rates of siderite and pyrite oxidation, r_{sidox} and r_{ndiox}, respectively (described in detail in the Supporting Information). Accounting for a nonbioavailable mass fraction allowed the model to capture the measured amount of nitrate remaining. The fitted model parameters suggest that only about 40−50% of the siderite was bioavailable. The limited siderite and pyrite oxidation, and thus limited bioavailability, could result either from limited dissolution of both minerals or from limited access of the cells to the mineral surfaces preventing direct oxidation of the solid Fe(II). In particular, the precipitation of Fe(III) (oxyhydr)oxides on the surface of the mineral particles could potentially limit or even prevent direct cell−mineral contact and therefore inhibit transfer of electrons from minerals to outer membrane proteins putatively participating in direct oxidation of Fe(II) such as cytochrome Cyc2.[32,33] Other potential factors limiting siderite and pyrite bioavailability could be the absence of defects and imperfections (steps and kinks) as their presence makes crystals more prone to dissolution and oxidation.[34,35] The precipitation of Fe(III) minerals close to the cells or at the cell surface can lead to cell encrustation,[36] which was also observed in our study (Figure S3), and can cause inhibition of the enzymatic cell activity or limit access to proteins or compounds other than enzymes that can mediate oxidation.[37]

Environmental Implications. Our study provides evidence for a direct microbial (enzymatic) contribution to oxidation of pyrite by an autotrophic nitrate-reducing enrichment culture, obtained from an organic-poor, pyrite-, Fe(II)-carbonate-, and nitrate-containing aquifer. Furthermore, microbially driven lithoautotrophic oxidation of bioavailable Fe(II) coupled to denitrification leading to Fe(III) formation does not seem to cause abiotic pyrite oxidation. Our results have important implications for predicting the fate of nitrate in environmental systems such as freshwater water bodies or sediments that are poor in organic carbon but contain other electron donors like Fe(II)- and S-phases. Specifically, it emphasizes the need of implementing direct enzymatic nitrate-dependent pyrite oxidation into reaction simulations when building field-scale models. The extent to which biologically catalyzed pyrite oxidation drives denitrification, however, will depend on the availability of other more preferential electron donors for nitrate reduction and may be greatly limited by the bioavailability of pyrite and/or dictated by the presence of specialized microbial communities that are able to facilitate the direct oxidation of pyrite as a solid Fe(II) source. Thus, future studies should aim to identify potential controlling factors determining solid-phase electron donor bioavailability such as crystallinity, the presence of trace metals, the presence of nonreducing ligands, and the role of surface availability for direct cell−mineral interactions to shed light on potential

electron transfer pathways between mineral surfaces and microbes.

■ ASSOCIATED CONTENT

Ⓢ Supporting Information

The Supporting Information is available free of charge at https://pubs.acs.org/doi/10.1021/acs.est.1c02049.

> Detailed information on Mössbauer spectra fitting parameters and reaction model parameters; additional SEM images of cell−mineral aggregates and NanoSIMS maps of the nonlabeled control setup; a plot showing reaction rates over time of incubation; a table with a mass balance summary of all experimental setups; and additional stoichiometric calculations (PDF)

■ AUTHOR INFORMATION

Corresponding Author

Andreas Kappler − *Geomicrobiology, Center for Applied Geoscience, University of Tuebingen, Tübingen D-72076, Germany;* ⓞ orcid.org/0000-0002-3558-9500; Email: andreas.kappler@uni-tuebingen.de

Authors

Natalia Jakus − *Geomicrobiology, Center for Applied Geoscience and Microbial Ecology, Center for Applied Geoscience, University of Tuebingen, Tübingen D-72076, Germany*

Adrian Mellage − *Hydrogeology, Center for Applied Geosciences, University of Tuebingen, Tübingen D-72076, Germany;* ⓞ orcid.org/0000-0003-2708-4518

Carmen Höschen − *Soil Science, TUM School of Life Sciences, Technical University of Munich, Freising-Weihenstephan D-85354, Germany*

Markus Maisch − *Geomicrobiology, Center for Applied Geoscience, University of Tuebingen, Tübingen D-72076, Germany*

James M. Byrne − *Geomicrobiology, Center for Applied Geoscience, University of Tuebingen, Tübingen D-72076, Germany; Present Address: Present address: School of Earth Sciences, University of Bristol, BS8 1RJ Bristol, U.K. (J.M.B.);* ⓞ orcid.org/0000-0002-4399-7336

Carsten W. Mueller − *Soil Science, TUM School of Life Sciences, Technical University of Munich, Freising-Weihenstephan D-85354, Germany; Present Address: Present address: Department of Geosciences and Natural Resource Management, University of Copenhagen, DK-1350 Copenhagen, Denmark (C.W.M.)*

Peter Grathwohl − *Hydrogeochemistry, Center for Applied Geoscience, University of Tuebingen, D-72076 Tübingen, Germany*

Complete contact information is available at:
https://pubs.acs.org/10.1021/acs.est.1c02049

Notes

The authors declare no competing financial interest.

■ ACKNOWLEDGMENTS

■ REFERENCES

(1) Tiedje, J. M. Ecology of Denitrification and Dissimilatory Nitrate Reduction to Ammonium. *Environ. Microbiol. Anaerobes* **1988**, *4*, 179−244.

(2) Kraft, B.; Tegetmeyer, H. E.; Sharma, R.; Klotz, M. G.; Ferdelman, T. G.; Hettich, R. L.; Geelhoed, J. S.; Strous, M. The Environmental Controls That Govern the End Product of Bacterial Nitrate Respiration. *Science* **2014**, *345*, 676−679.

(3) Nizzoli, D.; Carraro, E.; Nigro, V.; Viaroli, P. Effect of Organic Enrichment and Thermal Regime on Denitrification and Dissimilatory Nitrate Reduction to Ammonium (DNRA) in Hypolimnetic Sediments of Two Lowland Lakes. *Water Res.* **2010**, *44*, 2715−2724.

(4) Kuypers, M. M. M.; Marchant, H. K.; Kartal, B. The Microbial Nitrogen-Cycling Network. *Nat. Rev. Microbiol.* **2018**, *16*, 263−276.

(5) Kumar, S.; Herrmann, M.; Blohm, A.; Hilke, I.; Frosch, T.; Trumbore, S. E.; Küsel, K. Thiosulfate- and Hydrogen-Driven Autotrophic Denitrification by a Microbial Consortium Enriched from Groundwater of an Oligotrophic Limestone Aquifer. *FEMS Microbiol. Ecol.* **2018**, *94*, 1−13.

(6) Rivett, M. O.; Buss, S. R.; Morgan, P.; Smith, J. W. N.; Bemment, C. D. Nitrate Attenuation in Groundwater: A Review of Biogeochemical Controlling Processes. *Water Res.* **2008**, *42*, 4215−4232.

(7) Liu, T.; Chen, D.; Li, X.; Li, F. Microbially Mediated Coupling of Nitrate Reduction and Fe(II) Oxidation under Anoxic Conditions. *FEMS Microbiol. Ecol.* **2019**, *95*, 1−12.

(8) Hopwood, M. J.; Statham, P. J.; Skrabal, S. A.; Willey, J. D. Dissolved Iron(II) Ligands in River and Estuarine Water. *Mar. Chem.* **2015**, *173*, 173−182.

(9) Bhattacharyya, A.; Schmidt, M. P.; Stavitski, E.; Martínez, C. E. Iron Speciation in Peats: Chemical and Spectroscopic Evidence for the Co-Occurrence of Ferric and Ferrous Iron in Organic Complexes and Mineral Precipitates. *Org. Geochem.* **2018**, *115*, 124−137.

(10) Weber, K. A.; Picardal, F. W.; Roden, E. E. Microbially Catalyzed Nitrate-Dependent Oxidation of Biogenic Solid-Phase Fe(II) Compounds. *Environ. Sci. Technol.* **2001**, *35*, 1644−1650.

(11) Hayakawa, A.; Hatakeyama, M.; Asano, R.; Ishikawa, Y.; Hidaka, S. Nitrate Reduction Coupled with Pyrite Oxidation in the Surface Sediments of a Sulfide-Rich Ecosystem. *J. Geophys. Res. Biogeosciences* **2013**, *118*, 639−649.

(12) Schippers, A.; Jørgensen, B. B. Biogeochemistry of Pyrite and Iron Sulfide Oxidation in Marine Sediments. *Geochim. Cosmochim. Acta* **2002**, *66*, 85−92.

(13) Vaclavkova, S.; Jørgensen, C. J.; Jacobsen, O. S.; Aamand, J.; Elberling, B. The Importance of Microbial Iron Sulfide Oxidation for Nitrate Depletion in Anoxic Danish Sediments. *Aquat. Geochem.* **2014**, *20*, 419−435.

(14) Postma, D.; Boesen, C.; Kristiansen, H.; Larsen, F. Nitrate Reduction in an Unconfined Sandy Aquifer: Water Chemistry, Reduction Processes, and Geochemical Modeling. *Water Resour. Res.* **1991**, *27*, 2027−2045.

(15) Jørgensen, C. J.; Jacobsen, O. S.; Elberling, B.; Aamand, J. Microbial Oxidation of Pyrite Coupled to Nitrate Reduction in Anoxic Groundwater Sediment. *Environ. Sci. Technol.* **2009**, *43*, 4851−4857.

(16) Zhang, Y.-C.; Slomp, C. P.; Broers, H. P.; Bostick, B.; Passier, H. F.; Böttcher, M. E.; Omoregie, E. O.; Lloyd, J. R.; Polya, D. A.; Van Cappellen, P. Isotopic and Microbiological Signatures of Pyrite-Driven Denitrification in a Sandy Aquifer. *Chem. Geol.* **2012**, *300-301*, 123−132.

(17) Pauwels, H.; Kloppmann, W.; Foucher, J. C.; Martelat, A.; Fritsche, V. Field Tracer Test for Denitrification in a Pyrite-Bearing Schist Aquifer. *Appl. Geochem.* **1998**, *13*, 767−778.

(18) Schwientek, M.; Einsiedl, F.; Stichler, W.; Stögbauer, A.; Strauss, H.; Maloszewski, P. Evidence for Denitrification Regulated by Pyrite Oxidation in a Heterogeneous Porous Groundwater System. *Chem. Geol.* **2008**, *255*, 60−67.

(19) Visser, A. N.; Lehmann, M. F.; Rügner, H.; D'Affonseca, F. M.; Grathwohl, P.; Blackwell, N.; Kappler, A.; Osenbrück, K. Fate of Nitrate during Groundwater Recharge in a Fractured Karst Aquifer in Southwest Germany. *Hydrogeol. J.* **2021**, *29*, 1153−1171.

(20) Yan, R.; Kappler, A.; Muehe, E. M.; Knorr, K. H.; Horn, M. A.; Poser, A.; Lohmayer, R.; Peiffer, S. Effect of Reduced Sulfur Species on Chemolithoautotrophic Pyrite Oxidation with Nntrate. *Geomicrobiol. J.* **2019**, *36*, 19−29.

(21) Moses, C. O.; Kirk Nordstrom, D.; Herman, J. S.; Mills, A. L. Aqueous Pyrite Oxidation by Dissolved Oxygen and by Ferric Iron. *Geochim. Cosmochim. Acta* **1987**, *51*, 1561−1571.

(22) Bottrell, S. H.; Parkes, R. J.; Cragg, B. A.; Raiswell, R. Isotopic Evidence for Anoxic Pyrite Oxidation and Stimulation of Bacterial Sulphate Reduction in Marine Sediments. *J. Geol. Soc.* **2000**, *157*, 711−714.

(23) Boyd, E. S.; Hamilton, T. L.; Havig, J. R.; Skidmore, M. L.; Shock, E. L. Chemolithotrophic Primary Production in a Subglacial Ecosystem. *Appl. Environ. Microbiol.* **2014**, *80*, 6146−6153.

(24) Percak-Dennett, E.; He, S.; Converse, B.; Konishi, H.; Xu, H.; Corcoran, A.; Noguera, D.; Chan, C.; Bhattacharyya, A.; Borch, T.; Boyd, E.; Roden, E. E. Microbial Acceleration of Aerobic Pyrite Oxidation at Circumneutral PH. *Geobiology* **2017**, *15*, 690−703.

(25) Sand, W.; Gehrke, T.; Jozsa, P. G.; Schippers, A. (Bio)-Chemistry of Bacterial Leaching - Direct vs. Indirect Bioleaching. *Hydrometallurgy* **2001**, *59*, 159−175.

(26) Peiffer, S.; Stubert, I. The Oxidation of Pyrite at PH 7 in the Presence of Reducing and Nonreducing Fe(III)-Chelators. *Geochim. Cosmochim. Acta* **1999**, *63*, 3171−3182.

(27) Jakus, N.; Blackwell, N.; Osenbrück, K.; Straub, D.; Byrne, J. M.; Wang, Z.; Glöckler, D.; Elsner, M.; Lueders, T.; Grathwohl, P.; Kleindienst, S.; Kappler, A. Nitrate Removal by a Novel Lithoautotrophic Nitrate-Reducing Iron(II)-Oxidizing Culture Enriched from a Pyrite-Rich Limestone Aquifer. *Appl. Environ. Microbiol.* **2021**, AEM-00460.

(28) Ehrenreich, A.; Widdel, F. Anaerobic Oxidation of Ferrous Iron by Purple Bacteria, a New Type of Phototrophic Metabolism. *Appl. Environ. Microbiol.* **1994**, *60*, 4517−4526.

(29) Klueglein, N.; Kappler, A. Abiotic Oxidation of Fe(II) by Reactive Nitrogen Species in Cultures of the Nitrate-Reducing Fe(II) Oxidizer *Acidovorax* Sp. BoFeN1 − Questioning the Existence of Enzymatic Fe(II) Oxidation. *Geobiology* **2013**, *11*, 180−190.

(30) Schaedler, F.; Kappler, A.; Schmidt, C. A Revised Iron Extraction Protocol for Environmental Samples Rich in Nitrite and Carbonate. *Geomicrobiol. J.* **2018**, *35*, 23−30.

(31) Notini, L.; Byrne, J. M.; Tomaszewski, E. J.; Latta, D. E.; Zhou, Z.; Scherer, M. M.; Kappler, A. Mineral Defects Enhance Bioavailability of Goethite toward Microbial Fe(III) Reduction. *Environ. Sci. Technol.* **2019**, *53*, 8883−8891.

(32) Shi, L.; Dong, H.; Reguera, G.; Beyenal, H.; Lu, A.; Liu, J.; Yu, H. Q.; Fredrickson, J. K. Extracellular Electron Transfer Mechanisms between Microorganisms and Minerals. *Nat. Rev. Microbiol.* **2016**, *14*, 651−662.

(33) He, S.; Barco, R. A.; Emerson, D.; Roden, E. E. Comparative Genomic Analysis of Neutrophilic Iron(II) Oxidizer Genomes for Candidate Genes in Extracellular Electron Transfer. *Front. Microbiol.* **2017**, *8*, 1−17.

(34) Chandra, A. P.; Gerson, A. R. The Mechanisms of Pyrite Oxidation and Leaching: A Fundamental Perspective. *Surf. Sci. Rep.* **2010**, *65*, 293−315.

(35) Renard, F.; Putnis, C. V.; Montes-Hernandez, G.; King, H. E. Siderite Dissolution Coupled to Iron Oxyhydroxide Precipitation in the Presence of Arsenic Revealed by Nanoscale Imaging. *Chem. Geol.* **2017**, *449*, 123−134.

(36) Kappler, A.; Schink, B.; Newman, D. K. Fe(III) Mineral Formation and Cell Encrustation by the Nitrate-Dependent Fe(II)-Oxidizer Strain BoFeN1. *Geobiology* **2005**, *3*, 235−245.

(37) Miot, J.; MacLellan, K.; Benzerara, K.; Boisset, N. Preservation of Protein Globules and Peptidoglycan in the Mineralized Cell Wall of Nitrate-Reducing, Iron(II)-Oxidizing Bacteria: A Cryo-Electron Microscopy Study. *Geobiology* **2011**, *9*, 459−470.